Urban Air Vehicle implementation and limitations

Development of a new acoustic tool for the noise prediction

Gabriele Bossotto
gabriele.bossotto@tecnico.ulisboa.pt

Instituto Superior Técnico, Universidade de Lisboa, Portugal
Politecnico di Torino, Turin, Italy

November 2021

Abstract

This project presents the prediction and the optimization study of noise produced by rotors of a new concept of transport: UAV (Urban Air Vehicle). This project of UAM (Urban Air Mobility) evolved in the recent years due to the overcrowding of the cities' roads; this is a solution that at the same time brought up to light different issues and one of these, main theme of this document, is the noise pollution. However, the ability to rapidly assess the performance of these new generation of vertical lift vehicles, with sufficient fidelity, is a current weakness of this nascent industry. For this reason, the intention of this project is the prediction of the noise produced by the rotor itself, the study of minimization and optimization of the noise sources. For this purpose, is adopted an open-source suite of mixed-fidelity aerodynamics and aeroacoustics (FLOWUnsteady) simulations. This latter is able to fully characterize induced velocities across the stable region flow, where blade element momentum theory (BEMT) operates. This method is coupled with an aeroacoustics solver for tonal (FW-H code PSU WOP-WOP based on Farassat 1-A formulation) and broadband noise predictions (Brooks, Pope, and Marcolini (BPM) equations). To validate the data produced through this simulation and prediction program the thesis is divided in a computational and an experimental part. In the first part wings, body and rotating blades are modelled through a combination of panel, vortex lattice, lifting line, and blade elements. Meanwhile, the second part is the analysis of the same model elaborated by the software in an anechoic chamber, in order to validate the data. This comparison allowed to confirm the high fidelity of the computational method adopted and affirm the studied noise optimization method with the objective to guarantee the use of this new concept of transport in the classic city routine.
Keywords: UAM, Rotor noise, Noise prediction, Noise optimization

1. Introduction

Airbus and other companies have declared that by 2030, 60 % of the world's population will be urban [1]. In fact, the recent significant population growth is expected to create a real need for innovative mobility options as ground infrastructure becomes increasingly congested. The solution that leverages the airspace above cities could be safe, sustainable and convenient. For this reason, the classical ways of transport need to be substituted through the development of new and innovative technologies, such as Urban Air Vehicles (UAV). Noise generated by UAV has been identified as a critical factor in its development. It is reasonable to think this type of innovative transport could only be accepted and used by most of the world population if acceptable values of noise pollution are provided. For this reason, an accurate prediction of the level of generated noise is of utmost importance. The rotor noise is one of the most annoying sources of noise in the UAV and its prediction is a complex and computationally demanding task. Therefore, the present work aims at developing a methodology for the noise prediction, using a new open-source of mixed-fidelity aerodynamics and aeroacoustics (FLOWUnsteady) simulations with its flexibility and low computational cost. Noise prediction methods are subdivided into two broad groups: best practice methods and theoretical methods. Best practice methods rely mostly on measurement databases. On the other hand, theoretical methods rely on physical models to calculate the noise production and propagation [11]. Thanks to the efforts driven by the Federal Aviation Administration (FAA) and NASA to predict noise for single fly-over events, was developed the first computer code ANOPP. In the last decade of 20^{th} century several codes were implemented thanks to the development of computational fluids dynamics (CFD) leading to the development of ANOPP2, which partly uses computationally intensive higher

fidelity methods. Other software tools have also been developed by NASA such as Advanced Subsonic and Supersonic Propeller Induced Noise prediction program (ASSPIN), focused on propeller noise, which is based on Farassat's formulations, and MUTE, that is a cutting-edge methodology with the objective to predict in detail the rotorcraft noise at the expense of great computational resources. Moreover, it is also possible to mention the development of an aircraft noise computer program FLIGHT, at the University of Manchester. It contains an acoustics branch where the acoustics emissions rely mostly on source modelling.

2. Background

The most common and identifiable sources of rotors noise can be broadly divided into discrete-frequency (deterministic) and broadband noise components (non-deterministic). The discrete-frequency noise contains the deterministic components:

- **Thickness noise:** noise due to displacement of fluid by rotor blade;
- **Loading noise:** noise due to force exerted on the fluid by the rotor blade surface;
- **Blade vortex interaction noise (BVI):** impulsive loading noise due to a tip vortex impacting a following blade;
- **High-speed impulsive noise (HSI):** in-plane noise associated with high advancing tip speeds (transonic noise).

Broadband noise is the result of turbulent flow interactions on or near the blade surface and its current prediction methods are semi-empirical, so it depends on measured data to find the constants required in the model. The non-deterministic loading noise sources are [5]:

- **Turbulence ingestion noise**: unsteady loading noise due to ingestion of atmospheric turbulence into the rotor;
- **Blade wake interaction noise**: noise caused by blade interactions with rotor wake turbulence;
- **Blade self noise**: noise produced by scattering of turbulent flow over the blade trailing edge.

The direction of propagation of the different sources of noise are shown in figure 1.

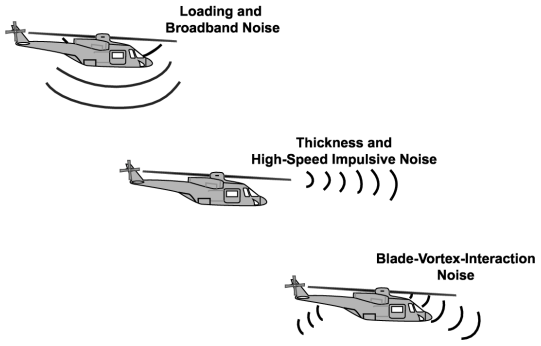

Figure 1: Primary rotor aerodynamic noise sources and associated directionalities for modern-day, full-scale helicopters, [5]

The acoustic analysis and optimization of UAV rotors is a complex process, and generally it involves several different methods. The first step of this computational chain is the calculation of the Aerodynamic loads through the implementation and cohesion of different methods:

- **Blade Element Momentum Theory (BEMT)** [2]: this iterative method is used to calculate the load distribution and for deriving the circulation along a vortex lattice representing the lifting surface;
- **Vortex Lattice Method (VLM)** [2]: used to elaborate the direction and strength of vortex particle being shed off the trailing edge and the velocity induced on nearby particles by the lifting surface;
- **Vortex Particle Method (VPM)** [2]: it is an unmesh-based solver well suited for the calculation of the wake-induced velocity and for the analysis of the unsteady wake dynamic.

The aerodynamic results of this first step are used as inputs for the second one, regarding the aeroacoustic analysis, which implements two different tools:

- **PSU-WOPWOP (PSW)** [8]: this tool, based on the Farasat's Formulation 1A, is used to analyse and predict tonal noise (deterministic);
- **Brooks, Pope and Marcolini (BPM)** [8]: it studies the broadband noise capturing noise from turbulent boundary layer edge, separation stall, tip vortex formation, laminar boundary layer vortex shedding, and trailing edge bluntness vortex shedding.

Finally, in the last step the data obtained previously are processed and plotted, in order to be displayed by the user.

2.1. Blade Element Momentum Theory (BEMT)

This theory is a model used to evaluate the performance of a propelling or extracting turbine based on its mechanical and geometric parameters as well as the characteristics of the interacting flow. This model results from the combination of two theories: the Blade Element Theory and the Momentum Theory. This latter is a global theory that adopts a macroscopic point of view to model the behavior of a column of fluid passing through a turbine, meanwhile the Blade Element Theory is a local approach that cuts the turbine blade into sections, the blade elements, each one of them being approximated by a planar model. This approach results in expressions of the forces exerted on the blade element, as functions of the flow characteristics and blade geometry. A combination of these two approaches was carried out in 1926 by Hermann Glauert. The purpose of the blade element momentum method is the computation of the induction factors a and a' and thus the steady loads and thus also the thrust and power for different settings of wind speed, rotational speed and pitch angle. These quantities are expressed as follows:

$$dT = \frac{1}{2}\rho B \frac{V_0^2(1-a)^2}{sin\Phi^2} cC_n dr \tag{1}$$

$$dM = \frac{1}{2}\rho B \frac{V_0(1-a)\omega r(1+a')}{sin\Phi cos\Phi} cC_t r dr \tag{2}$$

$$a = \frac{1}{\frac{4sin\Phi^2}{\sigma C_n} + 1} \tag{3}$$

$$a' = \frac{1}{\frac{4sin\Phi cos\Phi}{\sigma C_t} - 1} \tag{4}$$

where ρ is the air density, B is the number of blades, V_0 is the free-stream velocity, c the local chord of the blade, C_n is the coefficient of local normal force, Φ is the inflow angle, ω is the rotational velocity and C_t is the coefficient of local tangential force.

2.2. Vortex Lattice Method (VLM)

It is capable of accurately calculating the aerodynamic loads on rotary and fixed wing systems operating in incompressible flow with affordable computational costs. The VLM is based on the fluid surrounding the body surface that is assumed to be of inviscid, incompressible ($\nabla \cdot \mathbf{V} = 0$) and irrotational ($\nabla \times \mathbf{V} = 0$) over the entire domain. It represents the lifting surface as an area on which a grid of horseshoe vortices is superimposed, in particular case the rotor blades are regarded as lifting surface without thickness which is divided into quadrilateral singularities containing the constant strength vortex ring elements. For each horseshoe is elaborated the velocities induced at a specific control point using the law of Biot-Savart. A summation is performed for all control points on the lifting surface to produce a set of linear algebraic equations for the horseshoe vortex strengths that satisfy the boundary condition of no flow through the lifting surface. The vortex strengths are related to the surface circulation and the pressure differential between the upper and the lower part. The pressure differentials are integrated to yield the total forces and moments. Considering the different panels in which the lifting surface is divided and a point (x,y,z) of the m_{th} panel, the velocity induced at this point by the vortex representing the n_{th} panel will be designated as $\vec{V_{m,n}}$:

$$V_{m,n} = G_{m,n}\Gamma_n \tag{5}$$

where the influence coefficient $\vec{G_{m,n}}$ depends on the geometry of the n_{th} horseshoe and its distance from the control point on the m_{th} panel. Through the linearity of the governing equations it is possible to evaluate the velocities induced on the n_{th} control point adding together the $2N$ vortices:

$$\vec{V_m} = \sum_{n=1}^{2N} \vec{G_{m,n}}\Gamma_n \tag{6}$$

Anyway, in order to elaborate the resultant induced velocity at any point in space it is necessary to know the strength of the $2N$ horseshoe vortices (Γ_n), and for this reason it is used the boundary condition that the component of the induced velocity normal to the wing at the control point balances the normal component of the free-stream velocity. Applying the instantaneous zero normal flow boundary condition on the control point of each element, a set of algebraic equations for the unknown strength of vortices can be established

$$\begin{aligned} &\mathbb{G}\Gamma = \mathbb{V}_{\hat{n}} \\ &\Rightarrow \Gamma = \mathbb{G}^{-1}\mathbb{V}_{\hat{n}} \end{aligned} \tag{7}$$

where the matrix $\mathbb{G}$ is regarded the influence coefficient, and the $\mathbb{V}$ elements are referred to the normal components of the free-stream velocity [3].

2.3. PSU-WOPWOP (PSW)

It is a complete rewrite of the original WOPWOP code, utilizing object-oriented design principles and focusing on the prediction of the noise of maneuvering rotorcraft or any other moving body. The theoretical background of the new code PSU-WOPWOP is the same of the original one. Almost all actual rotor noise prediction tools, and also the one used in this study, are based on time-domain integral formulations of the Ffowcs Williams-Hawkings

(FW-H) equation. The FW-H equation is based on the Lighthill's acoustic analogy and it is an exact rearrangement of the continuity equation and the Navier-Stokes (N-S) equations into the form of an inhomogeneous wave equation [10]. The equations of mass and momentum conservation are the basis of the aerodynamic generation of sound. It is possible to combine these two equations considering a closed surface, obtaining an inhomogeneous wave equation that governs the propagation of the sound waves in a region exterior to the closed internal surface. After some manipulations of these two equations it is possible to obtain the FW-H equation:

$$\begin{aligned}&(\frac{\partial^2}{\partial t^2} - c^2\frac{\partial^2}{\partial x_i^2})(\overline{\rho - \rho_0}) = \\ &= \frac{\partial}{\partial t}[\rho_0 v_n \delta(f)] - \frac{\partial}{\partial x_i}[p_{ij} n_j \delta(f)] + \frac{\partial^2 \overline{T_{ij}}}{\partial x_i \partial x_j}\end{aligned} \tag{8}$$

In this equation $\overline{T_{ij}}$ is a generalized function equal to Lighthill's stress tensor, $T_{ij} = \rho u_i u_j + p_{ij} - c^2(\rho - \rho_0)\delta_{ij}$ outside any surfaces and equal to zero inside them. From the expression 8 it is possible to notice that the sound is generated by three different sources distributions:

- The first term is a monopole source frequently associated to the thickness noise;
- The second term is a dipole source associated to the loading noise;
- The last term is the quadropole source, associated to the HSI noise propagation, of strength density T_{ij} distributed along the whole exterior volume of the surface. It models the nonlinearity from local sound speed variation and finite fluid velocity in the region near the surface.

An integral form of the FW-H solution was developed by Farassat, called formulation 1A of Farassat, which neglects the quadropole terms because volume integrals are computationally expensive and PSU-WOPWOP neglets them. This formulation is able to describe the acoustic pressure fluctuation produced by an acoustic data surface given by the sum of the two contributions (thickness p'_T and loading p'_L):

$$p'(x,t) = p'_T(x,t) + p'_L(x,t) \tag{9}$$

where the thickness p'_T and loading p'_L contributions are calculated from:

$$\begin{aligned}&4\pi p'_T(x,t) = \int_{f=0}\left[\frac{\rho_0 \dot{v_n}}{r(1-M_r)^2}\right]_{ret} dS + \\ &+ \int_{f=0}\left[\frac{\rho_0 v_n}{r^2(1-M_r)^3}[r\dot{M_r} + c(M_r - M^2)]\right]_{ret} dS\end{aligned} \tag{10}$$

$$\begin{aligned}&4\pi p'_L(x,t) = \frac{1}{c}\int_{f=0}\left[\frac{\dot{l_r}}{r(1-M_r)^2}\right]_{ret} dS + \\ &\frac{1}{c}\int_{f=0}\left[\frac{l_r(r\dot{M_r} + cM_r - cM^2)}{r^2(1-M_r)^3}\right]_{ret} dS + \\ &+ \int_{f=0}\left[\frac{l_r - l_M}{r^2(1-M_r)^2}\right]_{ret} dS\end{aligned} \tag{11}$$

where $r = |x - y|$ and $(x,t),(y,\tau)$ are the observer and the source space-time variables, respectively, M_r is the Mach number of the point η in the radiation direction at time τ, S is the surface, the subscript ret refers to the retarded time, $l_r = l_i \hat{r_i}$ and $l_i = p_{ij} n_j$.

2.4. Fast Fourier Transforms (FFT) and Inverse FFT

A signal contains one or more frequencies, and it can be considered in the time domain or in the frequency domain; the conversion from time domain to the frequency domain is usually done using the Fourier Transform. In this study case, the signal is the acoustic pressure sampled over a finite time interval, so, it will be used a Discrete Fourier Transform (DFT). But its substantial computational cost can be reduced adopting an another method: Fastest Fourier Transform (FFT). The FFT is an efficient algorithm for computing the DFT and thanks to the lower number of computations it results to be more precise. In particular PSU-WOPWOP uses a package called FFTW (Fastest Fourier Transform in the West). When a 1-D array of real numbers is sent , x, this library returns a 1-D aray of complex numbers, X. The result of FFTW is used to calculate a complex pressure at each frequency bin. The units of complex pressure is Pascals.

2.5. Sound Pressure Levels (SPL)

The very small fluctuation in atmospheric pressure of the sound waves are the sources of noise received by human ear. The sound pressure is measured in a logarithmic scale called the decibel (dB) scale; this latter is defined by comparing sounds to a reference pressure of $p_0 = 20 \times 10^{-6} N/m^2$, value assigned to a SPL of 0.0 dB. The SPL in dB is computed by:

$$SPL(dB) = 10\log_{10}\left[\frac{[p^2]}{(20\times 10^{-6})^2}\right] \tag{12}$$

Each frequency range, either an octave band or an entire spectrum has a single SPL value associated with it. If the entire spectrum is sampled, the SPL returned is the overall sound pressure level (OASPL). However, the level of generated noise is subjective, so it is necessary to take into account the human ear. To overcome this problem A-weighting decibel (dBA) was created, whose correction can be applied to all the individual SPLs and OASPL. A-weighted sound pressure levels is the most common type of weighting.

2.6. **Brooks, Pope and Marcolini (BPM)**

This model was developed by Brooks Pope and Marcolini in 1989 for the prediction of the self-generated noise of an airfoil blade encountering smooth flow. This method is semi-empirical and based on previous theoretical studies and on the most comprehensive self-noise data set available. The BPM model includes five self-noise mechanisms for airfoil immersed in a flow due to the specific boundary-layer phenomena: boundary-layer turbulence passing the trailing edge (TBL-TE), separated-boundary-layer and stalled-airflow flow, vortex shedding due to laminar-boundary-layer instabilities, vortex shedding from blunt trailing edges, and the turbulent vortex flow existing near the tips of lifting blades. The predictions are matched with the data base from NACA 0012 airfoil blade sections of different sizes (chords from 2.5 to 61 cm) tested at wind tunnel speed up to Mach 0.21 (Reynolds number based on chord up to $3 \cdot 10^6$) and at angles of attack from 0° to 25.2°[4].

3. Implementation

FLOWUnsteady mechanism can be divided into steps, as observed in figure 2.

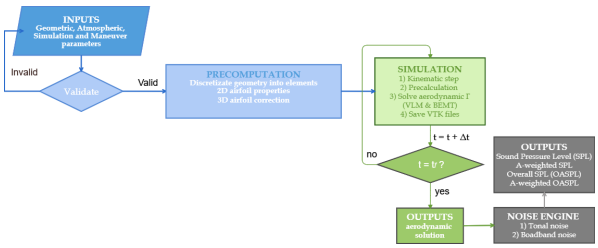

Figure 2: Computation diagram of FLOWUnsteady engine

3.1. **Inputs**

The geometry input specifications are defined through comma separated value (CSV) files that describe the airfoil, blade and rotor characteristics. For a whole definition of the geometry it is necessary a precise description of the structure. Taking into account the case of a single rotor model, it is request to the user to define as input the number of blades, radius of the tip and hub, chord distribution, pitch distribution, height of the leading edge with respect to the top face of the hub, sweep distribution, and the airfoil distribution from the root to the tip of the single blade. Together with the CSV geometric parameters, at the hypothetical user is request to define atmospheric parameters, simulation parameters (number of lattice elements, number of revolutions in the simulation, number of steps for each revolution, total time) and maneuver parameters (RPM trend, angle of tilting systems trend, velocity and angles of the whole vehicle trend).

3.2. **Precomputation**

The characteristics handled in the defined CSV files are used by the software XFoil in order to precompute the two-dimensional aerodynamic characteristics of each blade element at the corresponding local Reyolds number [6]. Subsequently, a Prandtl-Glauert compressibility correction is applied to lift curves, capturing compressibility effects. Both lift and drag curves are then treated to capture three-dimensional drag and stall-delay effects encountered in rotor blades and the Viterna method is applied to obtain post-stall $\pm 180°$ extrapolations of these curves. Following the different distribution defined in the CSV files, FLOWUnsteady is able to create the 3D geometry and generate the Vortex Lattice Method model, where each blade will be discretized into n horseshoes. FLOWUnsteady uses the generated three-dimensional geometry of the vehicle as spatial state variables (referred as G), along with the velocity of the vehicle V and angular velocity Ω. In this study, each blade of the propeller is modeled as a rotary lifting surface where the physics of interest have been broken down into three aspects: load distribution, blade-induced velocity, and wake-induced velocity. The load distribution is calculated through BEM theory and used for deriving the circulation along a vortex lattice representing the lifting surface. In turn, the vortex lattice is used as a framework for manipulating the rotating geometry, calculating the direction and strength of vortex particles being shed off the trailing edge, and calculating the velocity that the lifting surface induces on nearby particles. Since the vehicle is defined using just BEM theory and VLM, the wakes are assume quasi-steady. This means that at every time step of the simulation the wakes of VLM models are represented as rigid, semi-infinite filaments as represented in figure 3, and wakes of BEM models are obtained from a conservation of momentum assumptions. This quasi-steady approach allows to consider VLM-on-VLM and VLM-on-BEM wake interaction. A quasi-steady solver assumes that perturbations at the source of a wake-shedding surface immediately affect the entirety of the wake.

Therefore, wings are solved with the vortex lattice method while shedding a rigid semi-infinite wake. Rotors are solved through blade element momentum theory, without attempting to model the effects of wake interactions.

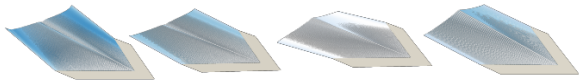

Figure 3: Heaving wing simulation with quasi-steady solver, in order to visualize the grid of horseshoes vortex superimposed on the wing structure

After the creation and discretization of the vehicle, the maneuver inputs, defined by the user, are implemented in order to create the maneuver desired that will be analysed during the simulation. The default maneuver used by FLOWUnsteady is kinematic, which means that RPM of the rotor system, angles of tilting systems, velocity and angles of the whole vehicle are defined through a function in time. In order to give the possibility at the hypothetical user to implement a dynamic maneuver a colleague of mine and I worked on the realization of a module in Julia language.

3.3. **Dynamic Maneuver**

In order to discuss about the dynamic maneuver implementation a quadcopter model with rotors arranged at the corners of a square body will be taken into consideration. This quadcopter will operate into two frames: the inertial frame and the body frame. The inertial frame is defined by the ground, since it is solidary with the Earth, with the gravity pointing in negative z direction. The body frame is defined by the orientation of the quadcopter, with the rotor axis pointing in the positive z direction and the arms pointing in x and y directions, as it is shown in figure 4.

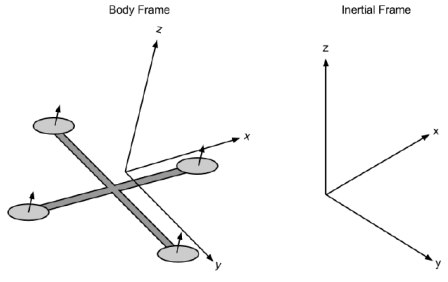

Figure 4: Quadcopter Body and Inertial frame

In the inertial frame the position and the velocity are defined as $x = (x, y, z)^T$, $\dot{x} = (\dot{x}, \dot{y}, \dot{z})^T$, respectively. Similarly, the roll, pitch, and yaw angles are defined in the body frame as $\theta = (\phi, \Theta, \psi)^T$, with corresponding angular velocities equal to $\dot{\theta} = (\dot{\phi}, \dot{\theta}, \dot{\psi})^T$. However, the angular velocity, ω, is different from $\dot{\theta}$ because ω is a vector pointing along the axis of rotation, while $\dot{\theta}$ is just the time derivative of roll, pith and yaw angles. For converting the angular velocities into the angular velocity vector, the following relation is defined:

$$\omega = \begin{bmatrix} 1 & 0 & -sin\theta \\ 0 & cos\phi & cos\theta sin\phi \\ 0 & -sin\phi & cos\theta sin\phi \end{bmatrix} \dot{\theta} \tag{13}$$

Where ω is defined in the body frame. As already done for the angular velocities, it is possible to relate the body and the inertial frames by a rotation matrix, R, which allows to go from the body frame to inertial frame. This developed dynamic code is merged with FLOWUnsteady code to use the forces and torques that are elaborated by applying BEMT and VLM to the model during the simulation. For this reason the matrix R is applied in order to map the thrust from the body frame to the inertial frame. In the inertial frame, the acceleration of quadcopter is due to the thrust vector (T_B), gravity (g), and linear friction (F_D). Hence, the linear motion can be summarized as

$$m\ddot{x} = \begin{bmatrix} 0 \\ 0 \\ -mg \end{bmatrix} + RT_B + F_D \tag{14}$$

where $\ddot{x}$ is the acceleration of the quadcopter and m is equal to the total mass of the model. The rotational equation of motion is derived from the Euler's equations for rigid body dynamics and expressed in the body frame. These Euler's equations are expressed in vector form

$$I\dot{\omega} + \omega \times (I\omega) = \tau \tag{15}$$

where I is the inertia matrix of the vehicle and τ is a vector of external torques. It is possible to rewrite this equation as

$$\dot{\omega} = \begin{bmatrix} \dot{\omega_x} \\ \dot{\omega_y} \\ \dot{\omega_z} \end{bmatrix} = I^{-1}(\tau - \omega \times (I\omega)) \tag{16}$$

Modelling the quadcopter as two thin uniform rods crossed at the origin with a point mass (motor) at the end of each, it is possible to get the final result for the body frame rotational equations of motion:

$$\dot{\omega} = \begin{bmatrix} \tau_\phi I_{xx}^{-1} \\ \tau_\theta I_{yy}^{-1} \\ \tau_\psi I_{zz}^{-1} \end{bmatrix} - \begin{bmatrix} \frac{I_{yy}-I_{zz}}{I_{xx}}\omega_y\omega_z \\ \frac{I_{zz}-I_{xx}}{I_{yy}}\omega_x\omega_z \\ \frac{I_{xx}-I_{yy}}{I_{zz}}\omega_x\omega_y \end{bmatrix} \tag{17}$$

Knowing the value of $\dot{\omega}$ it is possible to elaborate the angular velocity vector ω and consequently the angular velocity θ through the relation defined in

equation (13). Thanks to the equation (14) the acceleration vector $\ddot{x}$ is defined, so the velocity vector is calculated as $\dot{x} = \dot{x}_{prev} + dt \cdot \ddot{x}$, where dt is the time step, and $\dot{x}_{prev}$ is the previous value of the velocity vector; and through $\dot{x}$ is possible to compute the position of the quadcopter in each time step.
Through this dynamic implementation the hypothetical user can simulate the flight maneuvers of the vehicle varying the values of RPM, so of the thrust and torque produced; an example of vertical climb of a double rotor model is shown in figure 5. It is necessary to take into consideration that adjacent propellers are rotated in opposite direction. In this module, several advanced effects that contribute to the highly nonlinear dynamics of quadcopter have been ignored: the rotational drag forces, blade flapping and the surrounding fluid velocities is ignored since it is considered low [12].

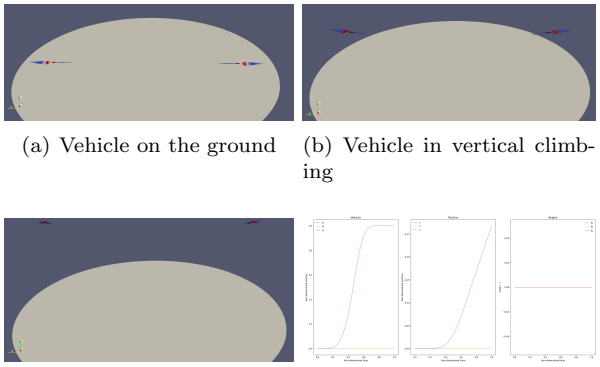

(a) Vehicle on the ground (b) Vehicle in vertical climbing

(c) End of the simulation (d) Velocity and position trend

Figure 5: Vertical climb of a double rotor model

3.4. **Simulation**

Once the 2D and 3D properties of the model are analysed and the maneuver is set up, it is possible to start the simulation and compute the aerodynamic loads acting along the structure and the induced velocities, as shown in figure 6.

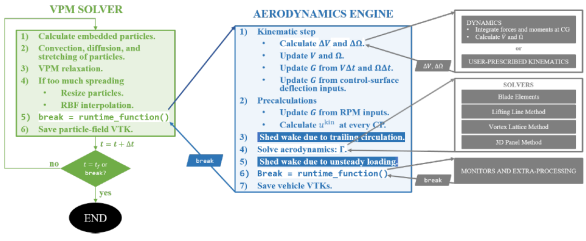

Figure 6: Flowchart of FLOWUnsteady framework, from [9]

The first step is the green box on the left, which is the VPM solver that drives the time stepping of the simulation. VPM is a mid-fidelity approach for modeling complex wake interactions. In the study conduced the VPM solver is not applied, only the BEM theory and VLM method are used to study the quasi-steady wakes. For this reason, the VPM solver continues to drive the time stepping of the simulation, but it is not direct implemented in the program. The green box calls another step of the flowchart in figure 6 represented by the light-blue box, which is called Aerodynamics engine. At this step the structure is moved in the simulation space, following the kinematic or dynamic rules. The geometry of the vehicle is shifted and rotated according to its translational and rotational velocity. First, velocities and vehicle angles changes, ΔV and $\Delta\Omega$, are either calculated from the kinematics or prescribed by the user. The state variables V and Ω are then updated, and the whole geometry is translated and rotated according to V and Ω. Since this process is repeated for each time step the time is updated $t_{sim} = t_{sim} + \Delta t$. Then the rotors are rotated according to RPM control inputs and the kinematic velocity V_{kin} of each control point (CP) of VLM systems are calculated; the horseshoes are recalculated with kinematic velocity and the previous circulation (Γ) solution is pasted to new system position after translation. Finally, it is applied the solver, which is itself divided into the following processes:

- the rotors are brought back to their initial positions at beginning of this time step before 'precalculations'. This is needed to avoid double accounting for the RPM when the solver is run;
- a initial solution of VLM systems is found using the free-stream velocity, V_∞, through the VLM method;
- the velocity induced, V_{ind}, by VLM systems on the rotor systems at each control point is calculated;
- the BEM theory is used to elaborate the circulation on each blade using the new $V_\infty + V_{ind}$ as velocity.

After this first step, where $n_t = 0$, it is calculated the solution of the wake system, treated as a VLM system, using $V_\infty + V_{ind}$ as velocity. Then, subsequently to these initialization of the systems used, the solver can continue with the following steps:

- the velocities induced by the wake-system on the VLM and rotor systems are elaborated;
- the velocities induced by the rotor systems on the VLM systems, and vice-versa, are calculated;

- it is elaborated the self-induced velocity by the rotor systems on themselves;
- The self-induced velocity of the rotor systems is subtracted from the total velocity, otherwise the solver will get on a positive-feedback instability;
- The VLM and rotor systems are solved, through VLM method and BEM theory, respectively, using the total velocity $V_\infty + V_{kin} + V_{ind}$;
- the rotors are rotated forward in order to undo the previous backward rotation.

All the solutions found are saved as previous solutions, since the whole light-blue box is repeated until the total time of the simulation is reached. Once all the aerodynamic solution are obtained, it is possible to proceed through the aeroacoustic computation. The aerodynamic solution and the analysis parameters are used to feed PSU-WOPWOP and BPM model.

4. Experiental Setup

In order to validate the accuracy of the code implemented, the computational noise data are compared to the experimental ones. The experiment is performed inside the Aeroacoustic Wind Tunnel located in the Aerospace Engineering Laboratory of Instituto Superior Técnico. The wind tunnel has a built-in Anechoic Chamber with a designed cut-off frequency of 200Hz. The equipment used in measurements conducted and the connections between them are shown in the scheme 7.

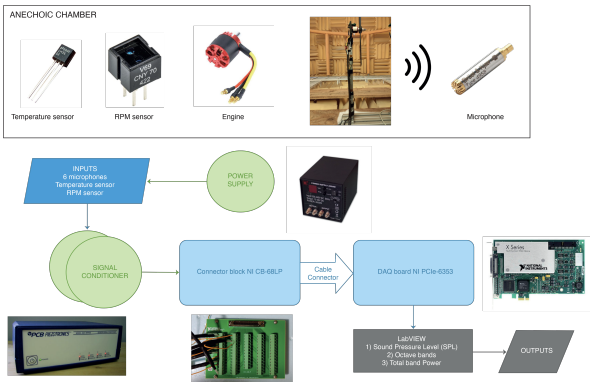

Figure 7: Equipment and connection of laboratory set up

Given the short time frame for this thesis and the pandemic contest, in this study are used the values collected by Pedro Miguel de Barros e Silva Duarte, who measured the noise produced by a single rotor made up by two blades, applying just 3 microphones at 45°, 0° and −45° with respect to the rotation plane of the rotor and at 2.3m from the hub, as shown in figure 8.

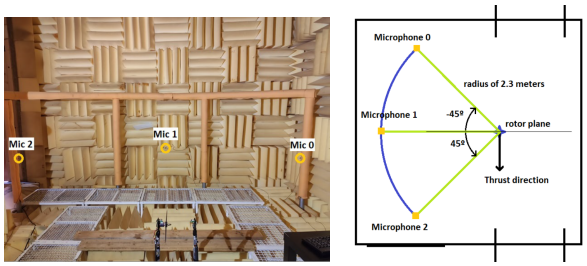

(a) (b)

Figure 8: The microphones positions in the anechoic chamber, from [7]

5. Results

The rotor tested in the experiment is called as "baseline" and in order to prevent any vibration of the rotor support and workbench the interval of rotation speeds tested was set to $1000 - 4000$ Rotations Per Minute (RPM), with variation steps of 500 RPM. Here only few of the plots obtained by the several comparisons done between the experimental and the computational values are presented. Analysing these graphs of figure 9, it is easily possible to state that the motor (orange line) and background (green line) have a substantial impact on the noise level received by the microphones for all the cases analysed at low RPM values. In order to understand the noise contribution given by the single rotor was made the difference between the noise values referring to the whole structure and motor ones, as shown in figure 10.

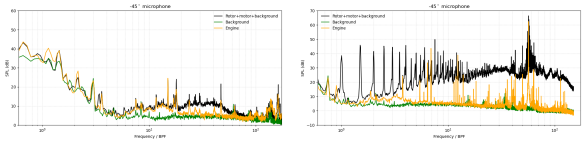

(a) RPM = 1000 (b) RPM = 4000

Figure 9: Whole structure, motor and background SPL spectrum at −45° at 1000 and 4000 RPM

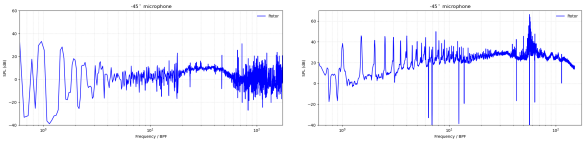

(a) RPM = 1000 (b) RPM = 4000

Figure 10: Difference between whole structure and motor SPL spectrum at −45° at 1000 and 4000 RPM

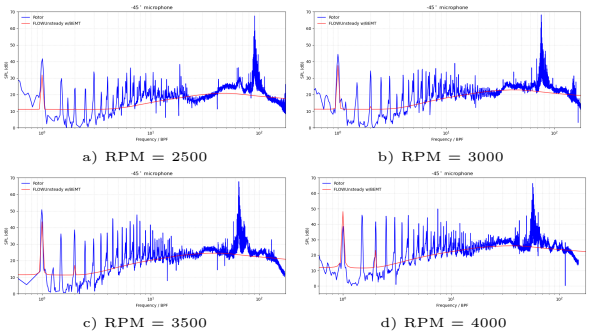

a) RPM = 2500 b) RPM = 3000

c) RPM = 3500 d) RPM = 4000

Figure 11: SPL spectrum comparison between FLOWUnsteady and experimental values at $-45°$ at $2500, 3000, 3500$, and 4000 RPM

The graphs shown in figure 10 highlight some possible resonance effects that happen between the sound waves produced by the motor and rotor, in fact for some frequencies the motor SPL value measured is higher than the whole structure, so through the difference the resultant rotor SPL value is lower than zero. The number of frequencies for which this effect happens decrease by increasing the RPM. For this reason, for the purpose of comparison are taken under consideration only the results obtained from the tests conduced at RPM values higher than 2500, where the percentage of negative rotor SPL cases is lower than 11% referring to the sampling frequency range of $20 - 20000$ Hz with a step of 2 Hz, so 9991 frequencies analysed in total. Hence, in figure 11 are shown the comparison conducted between the SPL spectrum predicted through the FLOWUnsteady code and the experimental ones.

As it is possible to observe in figure 11 the first BPF is well predicted and in general the trend of the SPL spectrum is followed at every frequency of the range considered. In each graph, for every rotation speed, a considerable peak always appears, between 7560 and 7570Hz , but it is not produced by the blades themselves; in fact, observing the orange lines in the figures presented in 9, it is reasonable to think that this noise peak is mainly generated by the motor when it is being powered to rotate and it was not possible to delete it completely.

5.1. **Parametric study**

Beyond the validation of the code accuracy, it is important to control the sensitivity and the main characters in the production of noise. For this reason, it is conducted a parametric study in order to evaluate the acoustic effects of varying the design and operating conditions of UAV rotors in hover. For this study the the DJI9443 rotor model for drones was taken into consideration. In order to conducted this parametric study was necessary to modify some of the main parameters that describe the rotor itself; after that, the whole simulation was run for all the cases analysed with 360 microphones located at $1.905m$ from the rotor hub, and compared with the baseline for seeing how the variation influenced the noise emission. In this study the chord and twist values of the blades were varied linearly along the span, firstly with a reduction, then applying an increment, more precisely doubling it; all these changes were applied keeping the other design parameters constant and at the same rotation speed of 5400 RPM. Figure 12 shows the influence of chord and twist changes on the thickness and loading noise sources in the OASPL directivity graphs.

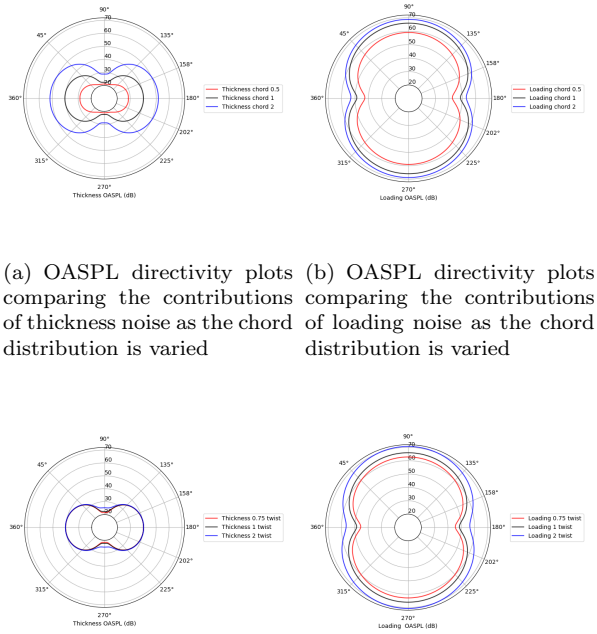

(a) OASPL directivity plots comparing the contributions of thickness noise as the chord distribution is varied

(b) OASPL directivity plots comparing the contributions of loading noise as the chord distribution is varied

(c) OASPL directivity plots comparing the contributions of thickness noise as the twist distribution is varied

(d) OASPL directivity plots comparing the contributions of loading noise as the twist distribution is varied

Figure 12: Thickness and loading noise directivity varying the chord and twist distribution

As it is possible to observe from figure 12 the chord increment leads to an increase of both thickness and loading noise, meanwhile the twist variation has influence in particular way on the loading contribution.

6. Conclusions

In the present work, the simulation engine FLOWUnsteady, developed at BYU's FLOW Lab and modified during the execution of the project, was used to predict the noise produced by the rotor of an unmanned aerial vehicle, since the size limitations of the 3D printer and wind tunnel of the Instituto Superior Técnico do not allow to test

UAV rotor model, the main subject of this work. The computational values obtained from the several simulation runs at different conditions of rotational speed and with different blades model were compared with the experimental ones in order to validate the software and analyse the agreement between them. The single component of the vehicle was tested in a controlled acoustic environment to characterize the primary noise generation mechanisms of the rotor, removing the noise generated by the presence of the electric motor and background noise. Computational results obtained for the simulation conduced at different rotation speed and captured from different microphones, located all around the rotation plane of the rotor in static hover conditions, revealed that the code performed well at predicting the first BPF acoustic amplitudes and SPL spectrum for these hover conditions, except for an underestimation of the noise captured by the microphone located in the rotation plane of the rotor (0°) due to a possible under estimation of the thickness noise and the neglection of the High-Speed Impulsive noise sources; both propagating in the rotational plane. The code used is flexible, with various possible inputs and options to select for running the computation, allowing the control of the simulations in detail. The rotor studied can be re-created in this virtual space defining its geometry inputs, position settings and atmospheric conditions. Then, the hypothetical user can define the simulation conditions and run the most disparate missions obtaining the deterministic and non-deterministic noise components from PSU-WOPWOP and BPM methods, respectively. In this way, it is possible to predict with a good agreement the noise pollution and optimize the blades in order to reduce it; contributing to the acceptance of the use of Urban Air Vehicle in the everyday life.

Acknowledgements

First of all i want to thank my family for supporting me along all these years of studying and for having believed in me without hesitation, even in the difficult moments, specially in these moments i would say, they helped me in all my decisions and doubts, making me to keep going. I would like to thank my thesis supervisors professors Fernando Lau and Frederico Afonso for all their teachings and guidance throughout the development of this thesis.

References

[1] Airbus. Urban air mobility: safe, sustainable and convenient. https://www.airbus.com/innovation/zero-emission/urban-air-mobility.html, Accessed on: 15 April 2021.

[2] Alvarez, E. J., and Ning, A. Development of a vortex particle code for the modeling of wake interaction in distributed propulsion. Atlanta,GA, June 2018. AIAA Applied Aerodynamics Conference. doi:10.2514/6.2018-3646.

[3] Bertin, John J. and Cummings, Russell M. *Aerodynamics for Engineers*. Pearson Education International, sixth edition, 2021. doi:10.1017/9781009105842.

[4] P. Bortolotti, E. Branlard, A. Platt, P. J. Moriarty, C. Sucameli, and C. L. Bottasso. Aeroacoustics noise model of openfast. Nrel/tp-5000-75731, NREL, Golden, CO: National Renewable Energy Laboratory, August 2020. doi:10.2172/1660130.

[5] K. S. Brentner and F. Farassat. Modeling aerodynamically generated sound of helicopter rotors. *Progress in Aerospace Sciences*, 39:83–120, April 2003. doi:10.1016/S0376-0421(02)00068-4.

[6] L. Clark. Faculty profile: Mark drela's research and his teaching. *AeroAstro*, pages 41–46, April 2005-2006. The Massachusetts Institute of Technology Department of Aeronautics and Astronautics.

[7] P. M. de Barros and S. Duarte. Novel concepts for noise mitigation of small uav rotors. Master thesis, Instituto Superior Técnico, October 2020.

[8] T. C. Eduardo Alvarez, Austin Schenk and A. Ning. Rotor-on-rotor aeroacoustic interactions of multirotor in hover. *Faculty Publications*, July 2020. 4053.

[9] Eduardo J. Alvarez. Quasi-steady aerodynamics solver for a high-fidelity controls framework. Technical report, Brigham Young University, Provo, Utah, 84602, 2020.

[10] W. J. E. Ffowcs and D. Hawkings. *Sound Generation by Turbulence and Surfaces in Arbitrary motion*. Philosophical Transactions of the Royal Society of London, Series A, Mathematical and Physical Sciences, 264(1151) edition, 1969. doi:10.1098/rsta.1969.0031.

[11] A. Filippone. Aircraft noise prediction. *Progress in Aerospace Sciences*, 68:27–63, March 2014. doi:10.1016/j.paerosci.2014.02.001.

[12] A. Gibiansky. Quadcopter dynamics and simulation. https://andrew.gibiansky.com/blog/physics/quadcopter-dynamics/, Accessed on: 8 July 2012.